

Article

Bending Properties of Cold-Formed Thin-Walled Steel/Fast-Growing Timber Composite I-Beams

Tianshu Chen ¹, Zhihua Chen ^{1,2}, Jiadi Liu ^{1,*} and Anling Zhang ¹

¹ Department of Civil Engineering, Tianjin University, Tianjin 300072, China; chentianshu@tju.edu.cn (T.C.); zhchen@tju.edu.cn (Z.C.); an_ling1997@tju.edu.cn (A.Z.)

² State Key Laboratory of Hydraulic Engineering Simulation and Safety, Tianjin 300072, China

* Correspondence: jdliu@tju.edu.cn

Abstract: A cold-formed, thin-walled steel/fast-growing timber composite system has recently been presented for low-rise buildings. It aims to increase the use of fast-growing wood as a green building material in structures, thus contributing to the transformation of traditional buildings. This study proposed a composite I-beam combined with fast-growing radiata pine and cold-formed thin-walled U-shaped steel. A four-point bending test was used to measure the bending properties of steel–timber composite I-beams under various connection methods. Based on experimental results, this study examined the specimen’s failure mechanism, mechanical properties, and strain development. In addition, a method for calculating flexural bearing capacity based on the superposition principle and transformed section method was suggested. It is evident from the results that fast-growing timber and cold-formed thin-walled steel can have significant composite effects. Different connecting methods significantly impact beams’ failure mode, stiffness, and bearing capacity. Furthermore, the theoretical method for calculating the flexural bearing capacity of composite beams differs from the test value by less than 10%. This paper’s research encourages the applications of fast-growing wood as light residential components, and it serves as a reference for the development, production, and engineering of steel–timber composite structural systems.

Keywords: bending performance; cold-formed thin-walled steel; composite beam; fast-growing timber; glue connection; mechanical connection



Citation: Chen, T.; Chen, Z.; Liu, J.; Zhang, A. Bending Properties of Cold-Formed Thin-Walled Steel/Fast-Growing Timber Composite I-Beams. *Forests* **2024**, *15*, 857. <https://doi.org/10.3390/f15050857>

Academic Editor: Milan Gaff

Received: 24 March 2024

Revised: 6 May 2024

Accepted: 10 May 2024

Published: 14 May 2024



Copyright: © 2024 by the authors. Licensee MDPI, Basel, Switzerland. This article is an open access article distributed under the terms and conditions of the Creative Commons Attribution (CC BY) license (<https://creativecommons.org/licenses/by/4.0/>).

1. Introduction

Steel, timber, and concrete are currently common structural materials. Steel has high strength and ductility. Cold-formed thin-walled steel is widely used because of its high strength-to-weight ratio and flexible cross-section. Unfortunately, it is limited due to the issue of stability, which can easily lead to buckling failure. Similarly, steel and timber both exhibit good seismic performance [1]. On the other hand, timber features light, high toughness, low energy consumption, and aesthetics [2]. Timber is wood that is processed into lumber with a regular shape. In China, *Pinus sylvestris*, spruce, larch, and Douglas fir are common wood species on the engineering market that produce highly graded and relatively high-quality lumber. Many studies have explored their use as sawn or engineered timber (CLT, OSB, LVL) in the main areas of building structures [3–6]. Fast-growing woods (such as radial pine, fir, and poplar) offer a potential application prospect in other raw woods. These fast-growing species have low to high densities (0.18~0.86 kg/m³) and fiber lengths similar to softwoods [7]. They have a short growth cycle (about 1 to 10 years), a short harvest time, a life expectancy of 20–25 years, and lower market prices than commercial tree species [8,9], and they have served as the main species planted in plantation forests [10]. Notably, many of these species can adapt to low-nutrient, dry, and erodible soils, providing additional financial and environmental benefits from harsher environments [11]. However, fast-growing species have more negative properties on wood

quality than non-fast-growing species, such as shorter fiber length, more significant growth stress [12], reduced strength and durability, more defects, loose and uneven texture, and deformation of logs or stock wood [13–15]. These characteristics limit their engineering applications in building structures.

To fully utilize the advantages of fast-growing woods and cold-formed thin-walled steel, one can combine the two materials to create a steel–timber composite system. In this structure, the steel may compensate for timber’s local defects and improve the overall mechanical properties and stability, while the timber serves as the steel’s lateral support and prevents the steel from buckling [16]. Furthermore, the timber also enhances the aesthetics of the building and the comfort of the dwelling [17]. Thus, the cold-formed thin-walled steel/fast-growing timber composite structure is a good choice for future village building growth. Among building elements, steel–timber composite beams have shown high potential in future engineering [18]. Compared to a steel beam, less material cost is needed to obtain the same bearing capacity [19]. Previously, steel–timber composite beams were created by applying steel elements to pre-existing timber constructions’ tension and compression zones. These composite beams successfully lower deflection and raised load capacity [20,21]. This reinforcement can be rod [22–24] and wire [25] and may be bonded or screwed steel plates [6,26–28]. Making steel and timber as a unified component is another design idea. Steel has significant bearing capacities, and wood laterally supports steel. The steel sandwich beam, sometimes called the Flitch beam, is the ancestor of this type of component [29]. This composite beam can also be built with steel sections [30,31]. Research and technical applications continually advance the innovations of the composite beam consisting of section steel and timber [32]. The steel types used in steel–timber composite beams are divided into cold-formed steel [33,34] and hot-rolled steel [35,36]. Hassanieh [35] tested the bending performance of H-shaped steel—LVL board composite beams (STC) fastened with adhesive, screws, or bolts. It was discovered that applying glue in conjunction with mechanical connectors can provide a near-full composite action in STC beams and significantly increase the initial stiffness of STC connections and STC beams. Kyvelou [37–39] proposed a composite beam consisting of oriented strand board (OSB) and cold-formed steel. Several studies were conducted on the beam’s overall structural performance to demonstrate the significant composite effect of the two materials. The results indicate satisfactory mechanical properties of the combined beam and the feasibility of potential engineering extension. Based on the current research, it can be found that the possibility of adapting fast-growing wood to these steels has been little presented and studied.

In addition to the material property, the connection performance between steel and timber also affects the mechanical property of the steel–timber composite beam [40]. Steel–timber composite beams are frequently connected using fasteners (bolts, screws), adhesives, etc. [41]. They can be separated into non-connection, partial composite, and complete composite styles according to the degree of inter-layer slippage [42]. While the mechanical connection is considered partially composite, the adhesive-bonded connection is thought to transmit force more continuously and thus is considered as a nearly complete composite [18]. The shear test results were commonly used in numerous studies [43–46] to characterize the stiffness, load-slippage, and bearing capacity of the connection interface in steel–timber composite beams. According to research by Hassanieh et al. [43], bolted connections demonstrated a ductile reaction when it came to the load slippage response of steel CLT connections. Compared to screw and bolt connections, adhesive connections were more rigid and had a greater peak load, but they also experienced brittle failure. In order to assess the stiffness, failure mode, and load slippage of shear connections between plywood (particle board) and steel using self-drilling self-tapping screws, Vella et al. [47] performed a push-out test. In an experimental study on the bolt and self-tapping screw connections of H-shaped steel larch-bonded wood composite beams, Yang et al. [48] found that self-drilling self-tapping screw connectors offer higher stiffness and more ductility compared to bolted connections. Chen et al. [49–51] showed that it is feasible to apply

self-tapping screw connections to cold-formed thin-walled steel fast-growing timber composite structural systems. They performed experimental and numerical studies on the performance of hexagonal self-drilling self-tapping screw connections and proposed a method for calculating screw bearing capacity and a simplified load-slippage model.

In the current study, steel–timber composite beams are examined, emphasizing their use in high-rise structures. Engineering timber and thick steel are the primary materials, whereas fast-growing wood is utilized less frequently. A single connection method, such as adhesive or bolt, is most common, with hybrid methods being rare. As rural houses undergo ecological and assembly transformations, combining cold-formed thin-walled steel and fast-growing timbers is an ideal option for low-rise dwellings [3]. This paper designed a cold-formed thin-walled steel/fast growing timber composite beam. Fifteen specimens were tested using the four-point bending method, exploring failure modes, mechanical properties, and strain distribution under various connections. The experiment results compared the performance of beams joined by self-tapping screws, bolts, adhesives, and hybrid connections. Additionally, the study considered interface slippage's impact on beam mechanics, proposing a simplified model to estimate elastic and ultimate flexural bearing capacity. This work aims to guide composite beam design and construction, advance steel–timber composite structures, and promote the use of fast-growing woods in lightweight residences.

2. Materials and Methods

2.1. Specimen Details

The 2700 mm × 138 mm × 214 mm (Length × Width × Height) cold-formed thin-walled steel/fast-growing timber composite beams are made up of two thin-walled U-beams (138 mm × 50 mm × 1.5 mm) and three timber boards (2700 mm × 138 mm × 38 mm), which are fastened together with glues, self-tapping screws, bolts, and timber screws. New Zealand radiata pine was chosen as the wood material, and the timber was cut into sawn boards and dried to reduce the moisture content to the required level. To investigate the impact of distinct connecting methods on the combined qualities of steel and wood in composite beams, five specimen groups—three parallel specimens for each group—were created as follows: S for self-tapping screw connection, B for bolt connection, A for adhesive connection, SA for screwed–adhesive hybrid connection, and BA for bolted–adhesive hybrid connection. Table 1 presents the connection parameters and description of each specimen group.

The U-section steel and timber boards were spliced and temporarily fastened with carpenter clamps during the processing and manufacturing of the steel–timber composite beams, following the bolt hole's marking and the strain gauge's installation. After that, H-section steel and wood were machined to have pre-drilled holes with a 6 mm diameter for the flange and a 7 mm diameter for the web. Bolts were then inserted from the timber's pre-drilled holes into the steel's pre-drilled holes, and a consistent pre-tightening force was applied. For the S group, after splicing and fixing, the self-tapping screws were driven from the designated location and secured with an electric drill to make the connection. For the A, SA, and BA groups with adhesive, the angle grinder with abrasive paper was used to polish the surface of the steel plate and wood for the specimen that was glued together to guarantee a tight fit between the two materials. After removing the steel's galvanized layer, 100% ethyl alcohol and gauze were used to clean the steel's surface. Steel and timber splicing surfaces were uniformly coated with two-component epoxy resin structural adhesive and then secured with carpenter clamps. Bolts or self-tapping screws were installed before the adhesive hardened. Then, the clamping degree of the woodworking was adjusted to maintain uniform clamping, the adhesive layer was left to solidify for 48 hours, and specimens were kept in conservation for at least seven days. The production and processing of beams of the BA group are depicted in Figure 1.

Table 1. Design description of steel–timber composite beams used in the experimental setup.

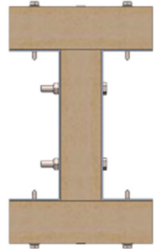
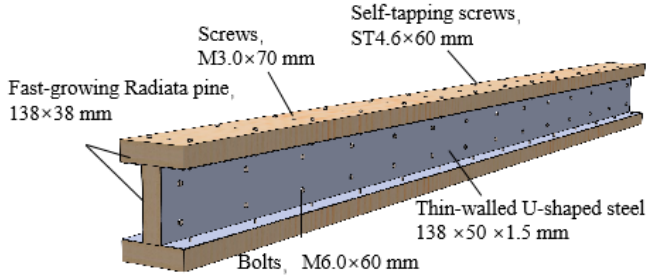
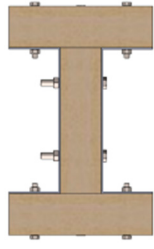
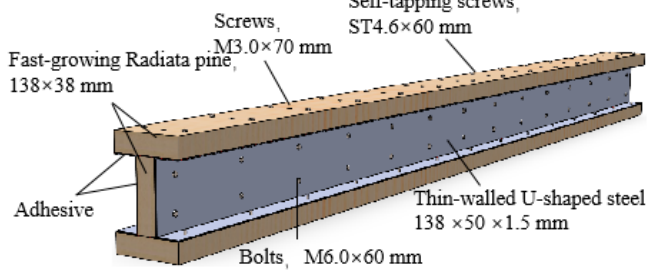

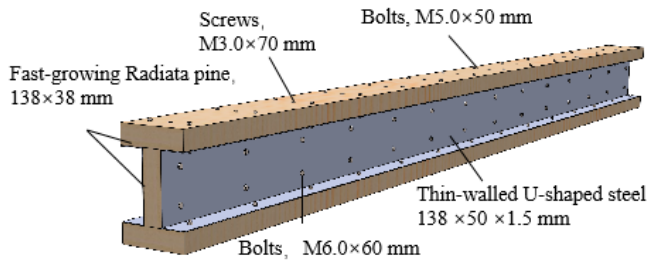
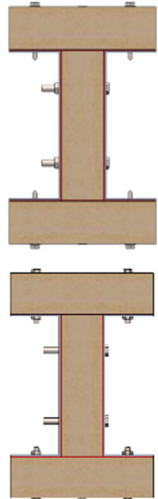
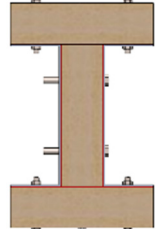
No.	Connection Method			Normal Section	Number	
	Steel–Timber Connection at Web	Steel–Timber Connection at Flanges	Timber–Timber Connection at Flanges			
S	Screwed	Screwed	Screwed			3
B	Bolted	Bolted	Screwed			3
A	Adhesive	Adhesive	Adhesive			3

Table 1. Cont.

No.	Connection Method			Normal Section	Number
	Steel–Timber Connection at Web	Steel–Timber Connection at Flanges	Timber–Timber Connection at Flanges		
SA	Screwed-adhesive	Screwed-adhesive	Screwed-adhesive		3
BA	Bolted-adhesive	Bolted-adhesive	Screwed-adhesive		3

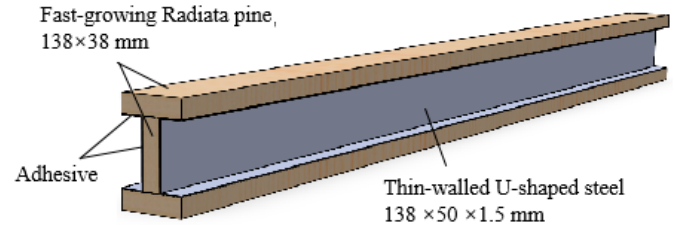
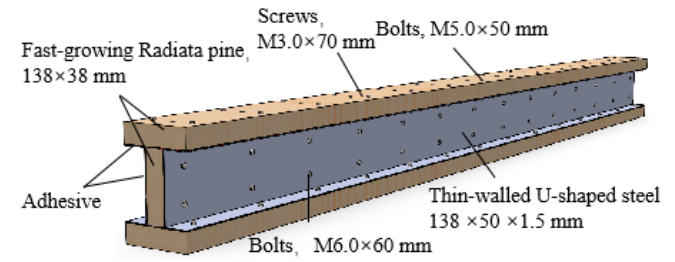




Figure 1. Manufacturing process.

2.2. Material Tests

2.2.1. Steel

Based on GB/T228.1-2021 [52], the steel properties were acquired as listed in Table 2 by taking samples from the same batch of 1.5 mm thick Q235B steel plates (Shelter, Wuqing District, Tianjin, China) used for composite beams. Three standard specimens were created to calculate the average value of the specimen groups. The steel material test is shown in Table 2.

Table 2. Steel material properties.

t (mm)	E_s (MPa)	ν_s	f_y^s (MPa)	f_u^s (MPa)
1.5	198.3	0.29	324.0	399.0

Note: t denotes the thickness of the steel, E_s denotes the elastic modulus, ν_s denotes Poisson's ratio, f_y^s denotes the yield strength, and f_u^s denotes the tensile strength.

2.2.2. Fast-Growing Timber Board

New Zealand radiata pine logs, aged approximately 8–10 years, were sourced to craft the timber boards for all beam specimens, which were prepared by grinding and polishing for this study. Based on GB 50005-2017 [53], GB/T 1943-2009 [54], GB/T 1939-2009 [55], GB/T 15777-2017 [56], and GB 1928-2009 [57], the elastic constant and compression strength of this fast-growing wood were obtained; see Figure 2. The samples for the wood material properties test were cut from sawn timber boards used to make composite beams (avoiding parts near the wood core). The compressive modulus of the wood was determined by calculating the ratio of stress to strain over a range of proportional ultimate stresses. The Poisson's ratio μ_{LR} , μ_{LT} and μ_{RT} was obtained by calculating the ratio of axial strain to transverse strain. Twelve samples of radiata pine, each measuring 60 mm × 20 mm × 20 mm, were prepared and weighed. The density of the wood was measured and calculated by means of an electronic scale (410 kg/m³, accuracy of 0.1 g). An induction wood moisture tester (accuracy ± 1.5%) measured the moisture content, and the average value of small pieces of wood sampled at different locations of the timber boards after drying was 11.8%, which complies with the requirements of GB/T 50329 [58]. The sapwood of radiata pine has a pH of 4.8, according to the information provided by the producer. All results are summarized in Table 3.

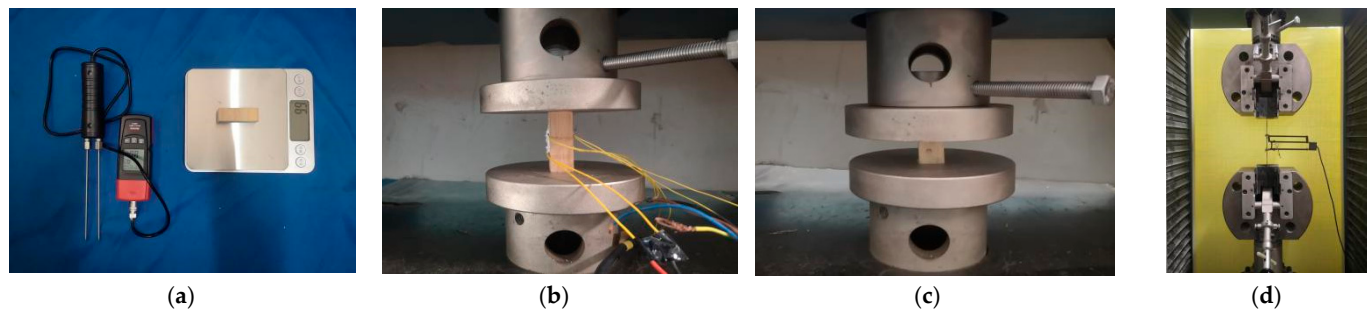


Figure 2. Material test. (a) Wood Moisture content and density test. (b) Wood elastic constant test. (c) Wood strength test. (d) Steel Material test.

Table 3. Timber properties test results.

Elastic Modulus (MPa)			Poisson's Ratio			Shear Modulus (MPa)			Compressive Strength (MPa)
E_L	E_R	E_T	μ_{LR}	μ_{LT}	μ_{RT}	G_{LR}	G_{LT}	G_{RT}	σ_L
6211	353	241	0.37	0.29	0.43	266	176	365	28.1

Note: σ_L denotes the longitudinal compressive strength. E_L , E_R , and E_T denote elastic modulus in three directions. μ_{LR} , μ_{LT} , μ_{RT} and G_{LR} , G_{LT} , G_{RT} denote the Poisson's ratio and shear modulus in three directions. L indicates longitudinal direction, R indicates radial direction, and T indicates tangential direction.

2.2.3. Adhesive

The glues used for steel–timber bonding consists of an epoxy resin (E44, 6101) and a hardener (WRS650) procured by Ailike Co., Ltd. (Ganzhou, Jiangxi Province, China) [59]. The adhesive is suitable for bonding wood and steel. The mixing ratio of the glues is 1:1. According to the information provided by the manufacturer, the initial curing time at a room temperature of 23 °C is 6 h, the total curing time is 24 h, and the steel–steel shear strength is 12 MPa. Given the lack of other relevant adhesive test results, we refer to the test information of the same component colloids. In refs. [60,61], tensile tests on standard dumbbell samples of the same component were used to measure the elastic modulus E_a , shear modulus G_a , and Poisson's ratio ν_a . Table 4 displays the mechanical properties of the two-component epoxy resin AB adhesive. Previously, the adhesive connection between cold-formed thin-walled steel and radiata pine timber was analyzed by tensile lap-joint tests, and their shear strength was measured [62].

Table 4. Adhesive properties.

Adhesive	E_a (MPa)	G_a (MPa)	ν_a (GPa)
Ailike	2330	890	0.37

2.2.4. Fasteners

The ST4.8 hexagon head self-tapping screw, which has a length of 60 mm and is composed of SWCH22A (carbon steel for cold pressing), was used for the steel–timber connection. The M3.0 cross countersunk head wood screws measuring 60 mm in length were used to join the flange timber and web timber. The shear and bending tests of self-tapping screws were carried out by GJB 715.24 A-2002 [63] and GB/T 232-2010 [64]. Three parallel experiments were conducted, and the average value was taken; specific details can be found in previous work [3,50]. The experimental results show that the average shear force of self-tapping screws is 7.6 kN, and the average ultimate bending moment is 11.34 kN·mm. The web adopted M6 (6 mm, grade 4.8) bolts, and the flange adopted M5 (5 mm, grade 4.8) bolts. The yield strength of the bolts is 320 MPa, and the ultimate strength is 400 MPa [3,65].

2.3. Test Setup and Instrumentation

A 500t electro-hydraulic servo control testing machine was used for the test. The test employed a distribution beam for vertical loading and a four-point bending loading method. The loading device is displayed in Figure 3a,c. The testing machine's pressure sensor detected the load. Five displacement gauges were positioned at the loading point, the middle of the beam, and the beam ends. The loading point deflection was measured with LVDT 1 and LVDT 2, the mid-span deflection was measured with LVDT 3, and the relative slippage between the steel and timber of the specimens was measured with LVDT 4 and LVDT 5. Additionally, as seen in Figure 3b, several strain gauges were placed on the timber boards of the upper and lower flanges, the upper and lower flanges of the steel, and the web of the steel to measure the strain change of the mid-span section. The specimen was preloaded to 15% of the predicted ultimate bearing capacity and then unloaded to ensure the test instrument operated correctly before loading. Formal loading involved applying the displacement at a constant axial compression rate of 1 mm/min. The application of a constant low displacement rate in the bending test is in consideration of the fact that the performance of the steel–timber composite beam is mainly affected by the connection and also for better observation of the interface morphology and characterization of the failure behavior of the composite beams [66]. The inclusion of an unloading phase in the loading process reduced the gap in the connection. Every second, the HP–AP data acquisition system observed and recorded the strain, displacement, and load. The test was terminated when the specimen's bearing capacity fell below 80% of the maximum load.

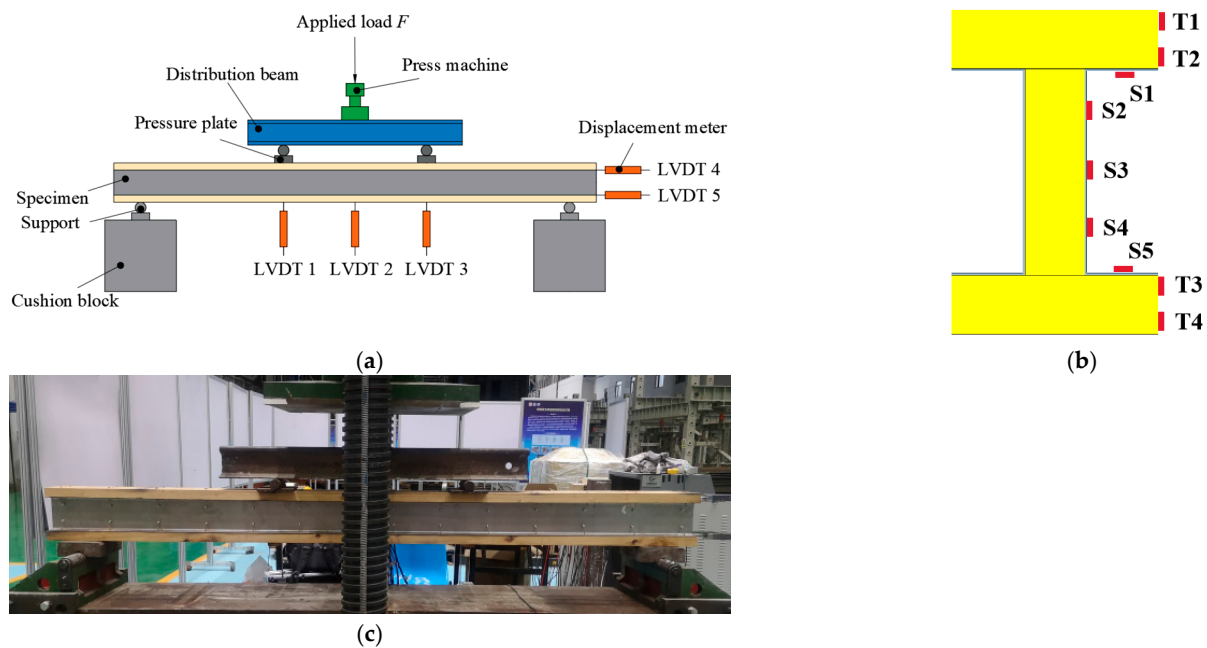


Figure 3. Experimental setup. (a) Layout of loading device and displacement meter. (b) Arrangement of strain gauge. (c) Field loading device.

2.4. Calculation Method for Flexural Bearing Capacity

The following three fundamental presumptions are put forward in order to calculate the bearing capacity of steel–timber composite beams under the limit state in this section:

- (1) The strain distribution across the mid-span section shows that the deformation of the mid-span section conforms to the plane section assumption;
- (2) The sliding behavior of the interface is neglected when the cold-formed thin-walled steel and timber boards are bonded;
- (3) The sliding behavior of the interface between cold-formed thin-walled steel and timber boards of composite beams is considered when they are mechanically connected. The

strain curvature of the flange and web is the same, and the additional stress of the section caused by sliding is distributed linearly.

The steel of the upper flanges of the mechanical connection beams will locally buckle as the beam approaches its maximum bearing capacity, causing the upper flange of steel plate to enter a state of yield and compression failure. In the case of the adhesive composite beams, the timber of the lower flanges is a failure in tension, and the steel stress in the upper flanges is still within the elastic range. There is no apparent buckling, the steel strain in the tensile zone exceeds the yield point. It can be regarded as the section's maximum capacity in the absence of any lateral torsional buckling or local buckling. The steel and timber are nearly complete composite. In other words, it can be considered that the timber retains its elasticity until the steel section reaches its elastic limit, at which point the bottom edge of timber boards meets the wood's strain or stress limit on the maximum load fiber. The steel goes into the yield state when the member starts to yield. Thus, in this study, the superposition approach is used to compute the ultimate bearing capacity of composite beams. In contrast, the conversion section method calculates composite beams' flexural elastic bearing capacity. Simultaneously, the bearing capacity is examined in relation to the steel-timber slippage between the upper and lower flanges. The centroid of the steel and wood members is situated in the exact location, and the beam in this study has two symmetrical sections.

The test results showed that when the composite beam was loaded to failure, the strain of the steel flange in the tension zone exceeded the yield point. To consider the plastic development of steel, the plastic ratio of the beams is proposed ($\gamma_s = 1.05$). In addition, slight debonding or cracking of the steel-timber interface at the upper flange occurred. Thus, timber's strength reduction coefficient $\gamma_t = 0.95$ is proposed [67]. Then, according to the superposition principle [68,69], the ultimate flexural bearing capacity of the normal section of the composite beam is obtained as Formula (1):

$$M_a^u = M_t^u + M_s^u \quad (1)$$

$$M_t^u = \gamma_t \sigma_t^u W_b \quad (2)$$

$$M_s^u = \gamma_s \sigma_s^u W_s \quad (3)$$

where M_a^u represents the ultimate flexural bearing capacity of the composite section, M_t^u represents the bearing capacity of the timber section, M_s^u represents the bearing capacity of the steel section, σ_t^u represents the tensile failure stress of the timber, and σ_s^u represents the failure stress of the steel of the flanges. W_b represents the section modulus of timber. W_s represents the section modulus of steel. In the mechanical connection specimens, when approaching the peak load, the section of the timber of the upper flanges is yield, and the steel of the flanges is fully buckled. Therefore, σ_t^u refers to the compressive yield stress of the timber of the upper flanges and σ_s^u refers to the yield stress of the steel of the upper flanges.

Mechanical connection composite beams slide at the interface, and the stress on the surface of the timber of the flanges is not equal to the stress on the surface of the steel flanges, resulting in strain difference on the upper and lower surfaces of the interface. Therefore, the bearing capacity M_f^u of a mechanical connection can be divided into the difference between the bearing capacity M_a^u of a complete shear connection and the additional bending moment ΔM_f generated by sliding. The calculation function (4) is as follows:

$$M_f^u = M_a^u - \Delta M_f \quad (4)$$

The elastic flexural bearing capacity of fully shear-connected composite beams can be calculated through the conversion section method [5] as Formula (5):

$$M_a^e = \sigma_s^y W_t^c + \sigma_s^y W_s = \sigma_s^y W_s^w + \sigma_s^y W_s^f + \sigma_s^y W_s \quad (5)$$

where W_f^c denotes the section modulus of timber transformed section, W_s denotes the section modulus of inertia of steel section, W_s^f denotes the section modulus of timber transformed section of the flanges and W_s^w denotes the section modulus of timber transformed section of the web.

In the elastic case, the yield capacity can be written as Formula (6):

$$M_f^e = M_a^e - \Delta M_f \quad (6)$$

The relationship between the elastic bending moment M and the load value P of the composite beams is calculated according to the following Formula (7):

$$M = Pa/2 \quad (7)$$

where a refers to the distance between the loading point and the proximal support. In addition, ΔM_f can be obtained in Formula (8) by referring to the relevant literature [70]:

$$\Delta M_f = E_s \Delta \varepsilon \left[\frac{h_s^2 A_f}{2h} + \frac{h_s h_f (A_f - A_w)}{3h} \right] \quad (8)$$

where E_s denotes the elastic modulus of steel, $\Delta \varepsilon$ refers to the interface strain difference, h refers to the total height of composite beams, h_f refers to the flange height of composite beams, h_s represents the web height of composite beams, A_f represents the cross-section area of flange of composite beams, and A_w denotes the cross-section area of flange of composite beams.

3. Test Results and Discussion

3.1. Phenomena and Failure Modes

During the test procedure, there were two common failure types for the specimens from Groups S and B (see Figure 4a). Failure mode I involved an extreme deflection of the beams that broke the wood fiber at the bottom of the timber in the lower flanges of the pure bending section. Early failure of some samples was due to defects such as knots in the wood on the web. It led to brittle or tensile fracture on the lower side, significantly diminishing the specimen's strength. Failure mode II involved deformation and buckling of the section steel upper flanges (between fasteners) in the pure bending section (Figure 4b). Simultaneously, most of the specimens' upper timber boards were crushed in the pure bending portion. Compression at the flaw caused cracking and damage to certain specimens, resulting in longitudinal cracks. The fasteners in this area underwent shear deformation due to the apparent slide of the end connection.

As shown in Figure 4c, the adhesive layer cracking caused the specimens in Group A to fail, and as the load increased, the debonding area progressively grew. A tiny region of steel buckling was frequently seen, and the upper flange was partially debonding. The abrupt release of stress was brought on by the localized cracking of the lower flange wood boards, which was accompanied by a violent debonding of the steel–timber interface. Usually, the lower flange's adhesive failure could expand to the bending–shear section. Specimen A-2 had a significant debonding area extending to the beam end. Thus, the end of the degumming specimen experienced some little slippage. The transverse fracture at mid-span failure and oblique fracture of the timber of the lower flanges constituted the ultimate failure. The specimens from Group SA and BA that failed are similar to those from Group A. There was a small-sized debonding at the upper flange, and the steel yielding accompanied the debonding zone (Figure 4d). The timber in the tensile region cracked, leading to adhesive failure. However, compared to the specimens of Group A, the debonding expansion range was substantially narrower because of the fasteners' limitations; see Figure 4e.

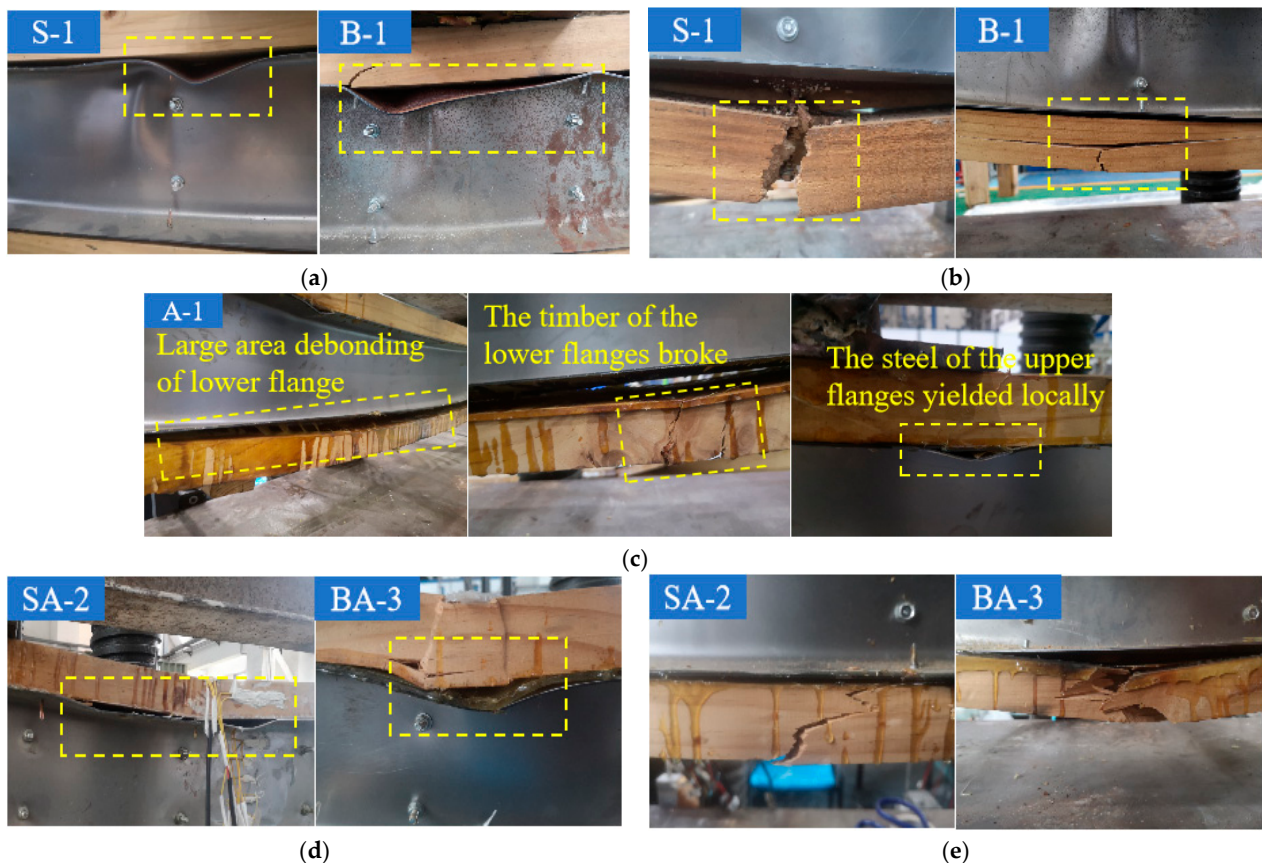


Figure 4. Failure phenomena of specimens. (a) The obvious buckling of steel in the upper flanges of specimens in Group S and Group B. (b) The split or fracture of timber at the lower flanges of specimens in Groups S and B. (c) Failure characteristics of Group A. (d) The steel buckling and local debonding of the upper flanges of specimens in Group SA and Group BA. (e) The fracture of the timber and local debonding at the lower flanges in Group SA and Group BA.

3.2. Bend Performance Analysis

3.2.1. Load-Displacement Curves

Four stages can be distinguished in the loading process for most specimens. Consider specimen S-1 as an example: at the early loading time, the beam entered the elastic working stage after a short initial slip stage. There was minimal specimen deformation, and a linear relationship existed between the load and the mid-span deflection. As the load increased, the specimen's deformation accelerated and reached the elastoplastic stage. The shear connection was deformed, the interface between the steel and the timber slid visibly, the upper flange of the cold-formed thin-walled U-shaped steel buckled and separated, and the upper flange of the composite beam extruded in the mid-span of the beam. The specimens underwent the plastic deformation stage at the late loading stage, mainly affecting Groups S and B. The steel started to buckle visibly, and the wood would occasionally crackle with the sound of broken fibers. In contrast to the preceding stage, the rate of load rise declined, the beams' mid-span deflection increased, and the curve tended to flatten. The timber on the upper flange of the composite beams exhibited complete compression yield in the pure bending section when the load was close to the peak value. The steel plate of the upper flanges also clearly showed signs of buckling, the shear connectors' deformation and the slippage of the steel–timber interface were more noticeable, and there was a more noticeable brittle sound from the fracture of the timber fiber. When the specimens finally reached the failure stage, the timber boards of the lower flange were entirely fractured, the curve abruptly dropped, and the timber boards of the upper flange were crushed at the

time of peak load. The beams were primarily in ductile failure mode. The load–midspan–displacement curve obtained from the test is shown in Figure 5.

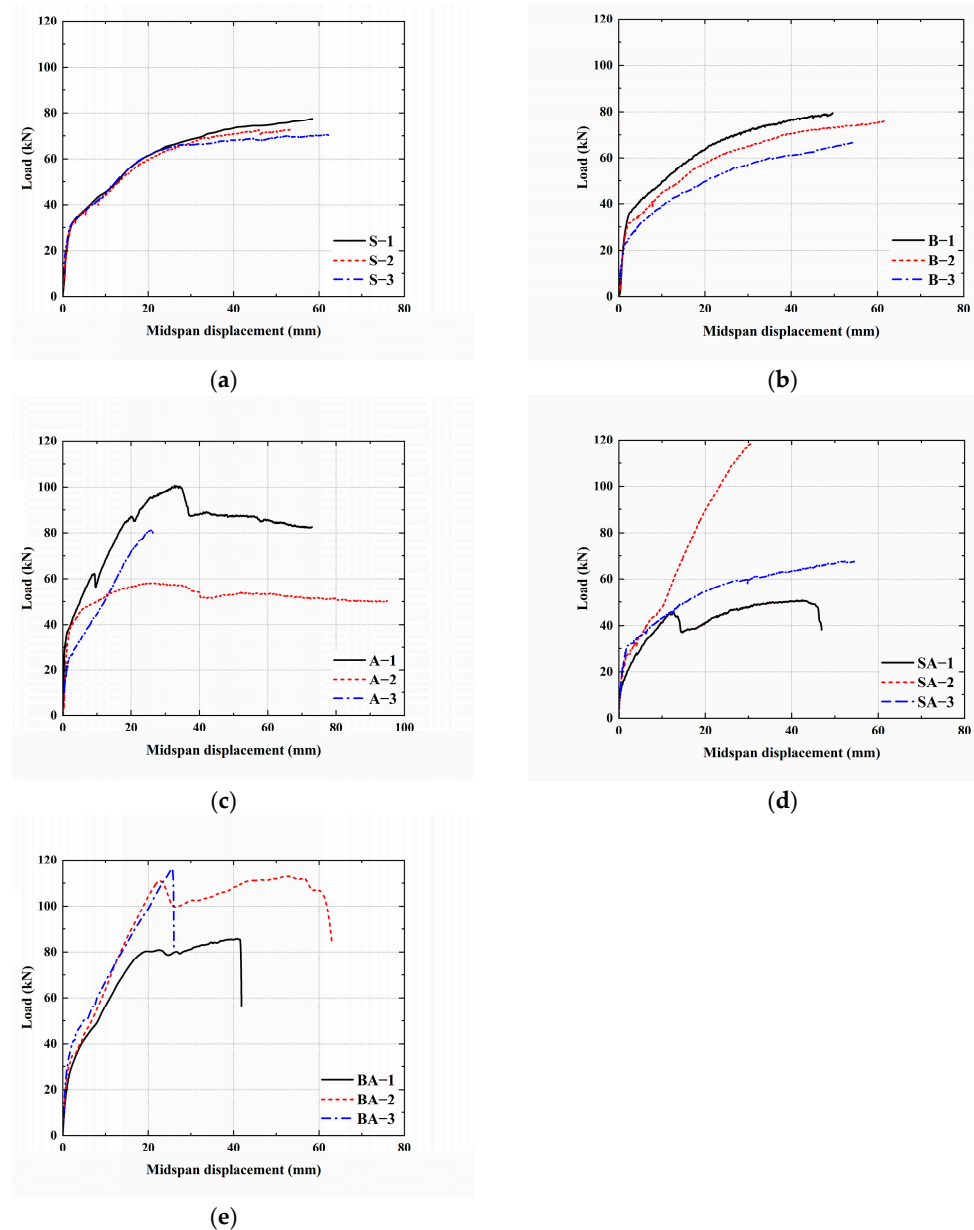


Figure 5. Load-midspan deflection curves for each group of specimens. (a) S group. (b) B group. (c) A group. (d) SA group. (e) BA group.

The load-midspan displacement curves for the mechanical connection groups (Group S and Group B) showed relatively consistent bearing capacity, stiffness, and development trends. However, the specimens (Group SA, BA, and A) using adhesives showed some differences in strength and displacement, and the curves have no significant inflection points. It was caused by the artificially treated adhesive interface's variations in adhesive strength and bonding quality. Failure of the adhesive in specimen A-2 was abrupt and global, resulting in loss of combined action and significantly lower peak bearing capacity. SA-1 and SA-3 show that the self-tapping screw driving process is more likely to degrade the quality of the adhesive layer before the adhesive cures than placing the bolt. It is a challenge to manage the interface's initial interference. The screws could not be adjusted to ensure uniform curing by adjusting the preload. Conversely, bolts make it easier to

provide and maintain (and later adjust) this tightening force during the fabrication of the adhesive layer.

Specifically, the load–midspan displacement curve of the A-2 specimen entered the yield stage prematurely. Due to the premature overall debonding of the adhesive layer from the web and lower flange, the load of the specimen rapidly peaked and declined. In contrast to the ideal curve development of the SA-2, BA-2, and BA-3 specimens when adequately prepared, the load-carrying performance of the SA-1 and SA-3 specimens is lower than expected. The brittleness crack at the edge of the tensile flange timber caused the expectant failure of SA-2 and BA-3. However, the curves of the less desirable specimens experienced more plastic development, illustrating their incomplete composite interfaces (similar to Groups B and S); i.e., the adhesive layer failed quickly upon the onset of loading, which determines a low degree of composite effect in the late period of loading process. The curve of SA-3 shows similarities with those of Group S, suggesting that the beam experiencing bond failure quickly transformed into screws as the dominant connection transferring the forces, exhibiting ductile damage characteristics. The late growth of the SA-1 curve, which quickly peaked and declined, was due to the premature destruction of timber boards of lower flange, which underwent a relatively rare defect-induced long axial through-cracking accompanied by delamination of the timber.

Despite rigorous pre-treatment to ensure bonding quality, two possible reasons can lead to premature bond failure. Firstly, some fast-growing timber boards have initial bending or torsional deformation. Although G-shaped fixtures straighten the boards to ensure the steel is tightly adhered to the timber, it is impossible to avoid initial internal stresses at the adhesive layers, particularly peeling stresses. The uneven texture of fast-growing wood results in inconsistent deformation at the various locations under humidity changes during storage, as shown in Figure 6 below. The second reason is that wood knots and other significant initial defects of timber are present at the bonding surface. It causes stress concentration in the timber under load. It may also lead to the concentrated shear stress or peeling stress of the adhesive layer, resulting in premature failure of the adhesive layer and rapid expansion of the range of debonding area.

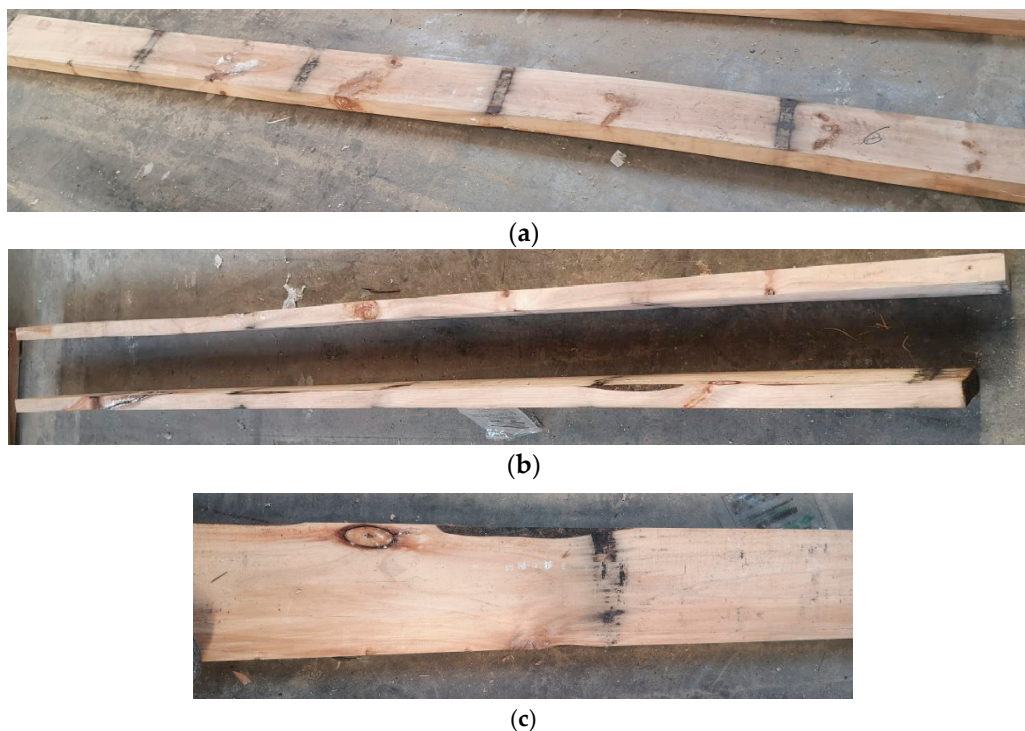


Figure 6. Timber defects that may affect bonding quality. (a) Initial bending deformation of timber boards. (b) Small torsional deformation of timber boards. (c) Wood knots on bonded surfaces.

3.2.2. Bearing Capacity

Table 5 displays the mechanical properties of all specimens of the five groups. For Group S and Group B with small discreteness, the average value of the parallel specimens was taken for each evaluation indices during the comparative analysis of mechanical properties. For other groups of specimens that have some discreteness owing to the influence of adhesive quality and natural defects of timber, the test results of specimen A-1 were taken for group A, the test results of specimen S-2 were taken for group SA, and the test results of specimen BA-3 were taken for group BA. A comparison of the results of all the groups is shown in Table 6.

Table 5. Test results of each group.

No.	P_y (kN)	Δ_y (mm)	P_{max} (kN)	Δ_u (mm)	β	K_e (kN/mm)
S-1	31.76	2.20	77.46	58.23	26.47	14.44
S-2	31.25	2.11	72.70	52.82	25.03	14.81
S-3	31.40	2.10	70.55	60.88	24.49	14.95
B-1	32.75	1.98	79.52	49.01	24.75	16.54
B-2	31.45	2.30	75.99	60.86	26.46	13.67
B-3	23.52	2.01	66.65	53.93	26.83	11.70
A-1	35.53	1.23	100.10	32.65	23.39	28.89
A-2	38.02	2.10	58.12	24.67	11.75	18.10
A-3	25.95	2.13	81.46	25.96	12.19	12.18
SA-1	20.54	2.22	50.49	46.86	21.11	9.25
SA-2	26.20	1.35	117.99	28.75	21.30	19.41
SA-3	31.12	5.85	67.46	55.01	9.40	5.32
BA-1	28.89	1.83	85.82	41.69	22.78	15.79
BA-2	32.89	1.72	112.96	23.12	13.44	19.12
BA-3	35.73	1.52	117.79	25.94	17.07	23.51

Note: P_y denotes the yield load. Δ_y denotes the yield displacement. P_{max} denotes the peak load. Δ_u denotes the displacement corresponding to the peak load. β denotes the ductility coefficient. K_e denotes the initial stiffness.

Table 6. Comparison of results between each group.

No.	P_y (kN)	Δ_y (mm)	P_{max} (kN)	Δ_u (mm)	β	K_e (kN/mm)
S-ave	31.47	2.14	73.57	57.31	25.33	14.73
B-ave	28.65	2.10	74.05	54.60	26.01	13.97
A-1	35.53	1.23	100.10	32.65	23.39	28.89
SA-2	26.93	1.35	117.99	28.75	21.30	19.95
BA-3	35.73	1.52	117.79	25.94	17.07	23.51

The findings demonstrate that, compared to Group S and Group B specimens, the ultimate bearing capacity of Group A specimens increased by 36.06% and 35.18%, respectively. It suggests that the adhesive connection was superior to the mechanical connection in the composite effect. A single fastener connection could have stabilizing combination effects of beams, as demonstrated by the generally consistent bearing capacity, rigidity, and development process of the bolt connection specimen (Group B) and screw connection specimen (Group S).

The strength of steel and timber can be fully utilized through the hybrid connection of adhesives and fasteners, significantly increasing the ultimate bearing capacity of composite beams. The specimens A-1, SA-2, and BA-3 showed similar curve development trends during the elastic and early plastic stages. However, the debonding of A-1 is more significant than the BA-3, and the stiffness and bearing capacity of the specimens started to decline slightly. The bearing capacity of the BA-3 specimen was 59.07% higher than in Group B. Though the elastic bearing capacity at the initial stage of the SA specimen was not high, the SA-2 specimen had a bearing capacity 60.38% greater than that of the S

specimens. It is evident from comparing the best adhesive specimens, A-1, SA-2, and BA-3, that the hybrid connection improved the ultimate bearing capacity by 18% compared with the adhesive connection. SA-2 and BA-3 exhibit a similar bearing capacity of 117 kN at optimal connection quality.

3.2.3. Stiffness

The yield displacement Δy is defined as the initial inflection point of the load-displacement curve. For the curve where the inflection point was negligible, the yield point is found using the farthest point method [71,72]. The initial stiffness K_e of the beam was obtained by taking the slope of the line between the yield point and the original point. Table 5 presents the results of K_e . In the A, BA, and SA groups, the adhesive connection offered a complete cross-section composite effect, which could fully play the role of steel and timber's resistance to deformation, resulting in a high degree of rigidity during the elastic stage. However, the stiffness at the elastic stage was lower in the S and B groups because the fastener connection was localized and had a low combination efficiency. SA-2 and BA-3 had stiffness values that were 35.4% and 68.3% greater, respectively, compared to screw and bolt specimens in Group B and S. The hole in the hybrid connection decreased the area of the initial adhesive interface and weakened the adhesive's full-section composite initially. Therefore, compared with the specimens of A-1, the stiffness values of BA-3 and SA-2 were slightly reduced.

3.2.4. Ductility Analysis

The ductility coefficient β is defined as the displacement ratio corresponding to the point after the peak load of 80% of the peak load and yield point. This factor is calculated as Formula (9):

$$\beta = \frac{\Delta u}{\Delta y} \quad (9)$$

where Δu refers to the displacement of the point after the peak load of 80% and Δy refers to the displacement of the yield point.

Table 5 presents the results, indicating that Group S and Group B had high ductility (25.33 and 26.01), and the results had a limited dispersion among the parallel groups. The evident compressive plastic deformation of the timber of the upper flanges of these specimens illustrated the ductile failure characteristics. The ductility of the adhesive specimen was less than that of the fastener-connected beams, suggesting that the upper timber's plastic characteristics are only limitedly utilized in the adhesive connection. The failure manifests a sharp decline in bearing capacity after the timber of the lower flanges initially broke. Compared to the fastener, the adhesive has a more substantial composite effect. The overall strength and ductility were reduced with a more complete connection due to the excessively high local stiffness. Additionally, the beams' strength might be lost early before wood damage if the shear connections could not withstand slippage. Simultaneously, the ductility of the A, BA, and SA groups was high discreteness due to differences in bonding quality.

3.2.5. Load-Strain Response

Figure 7 depicts typical load-strain curves for the beams' midspan section. The location and name of each strain gauge are shown in Figure 3b. During the test process, it was observed that the upper part of the composite beam was in compression, while the lower part was in tension. The point of zero strain was located in the center of the section. The upper side of the web timber was under compression, whereas the lower side was under tension. For most beams, strain was directly proportional to load in the linear elastic range when the load was less than 30 kN. Once the load exceeded approximately 30 kN, the specimen entered the elastoplastic range, and the strain varied nonlinearly with the load. When the bearing capacity surpassed 80% of the peak load, the bearing capacity curves of S-2, B-1, and A-1 exhibited significant growth or regression features. The maximum strain of the steel in the elastic stage was typically observed at the steel flanges, while a maximum

strain of 3.7×10^{-3} might be attained at the web in the plastic stage. The top surface of the timber board in the upper flanges experienced the highest strain, which was 6.5×10^{-3} . The curve regression and nonlinear expansion in the late loading stage in Groups B and S indicate the buckling of steel. The flanges' timber was mainly stressed during this phase until it either failed in tension or compressed to yield. In groups SA and BA, the linear growth at each position approached the peak load, explaining the tensile failure of the timber in the lower flanges and nearly elastic behavior at other positions.

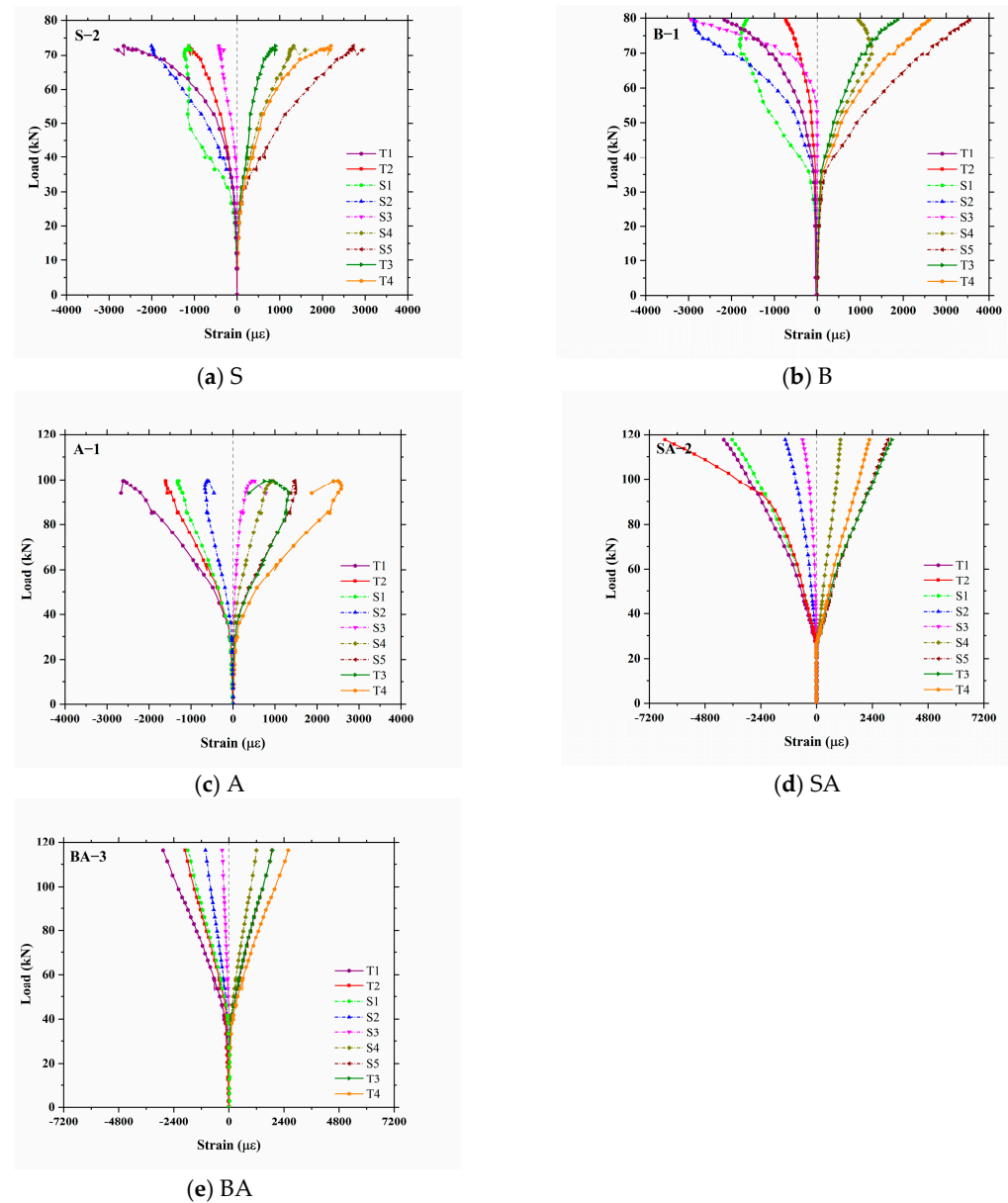


Figure 7. Load–Strain Curve.

The strain distribution along the heights of the midspan sections of the composite beams under various loads is depicted in Figure 8. Before loading, the load–strain curves for steel and timber are linear along the heights, consistent with the plane section assumption that the point of zero strain is close to the section's center. The strain on the flange's outer surface could represent the strain on the flange connection surface due to the relatively thin steel flange. The strain along the axial direction was measured for steel and wood near the joint interface of the flange. Relative slippage was minimal at the beginning, so it could be ignored. During the entire stage of Group B and Group S, the strain curve reached a rapid

growth stage, presenting at the later stage of the other groups (when the adhesive layer was damaged). At this interface, the strain difference increased as the load increased, and the amplitude of the increase also increased. It suggests a considerable amount of relative slippage between the steel and timber of the flanges with different elastic modulus because of the locally coupled connection between the steel and the timber.

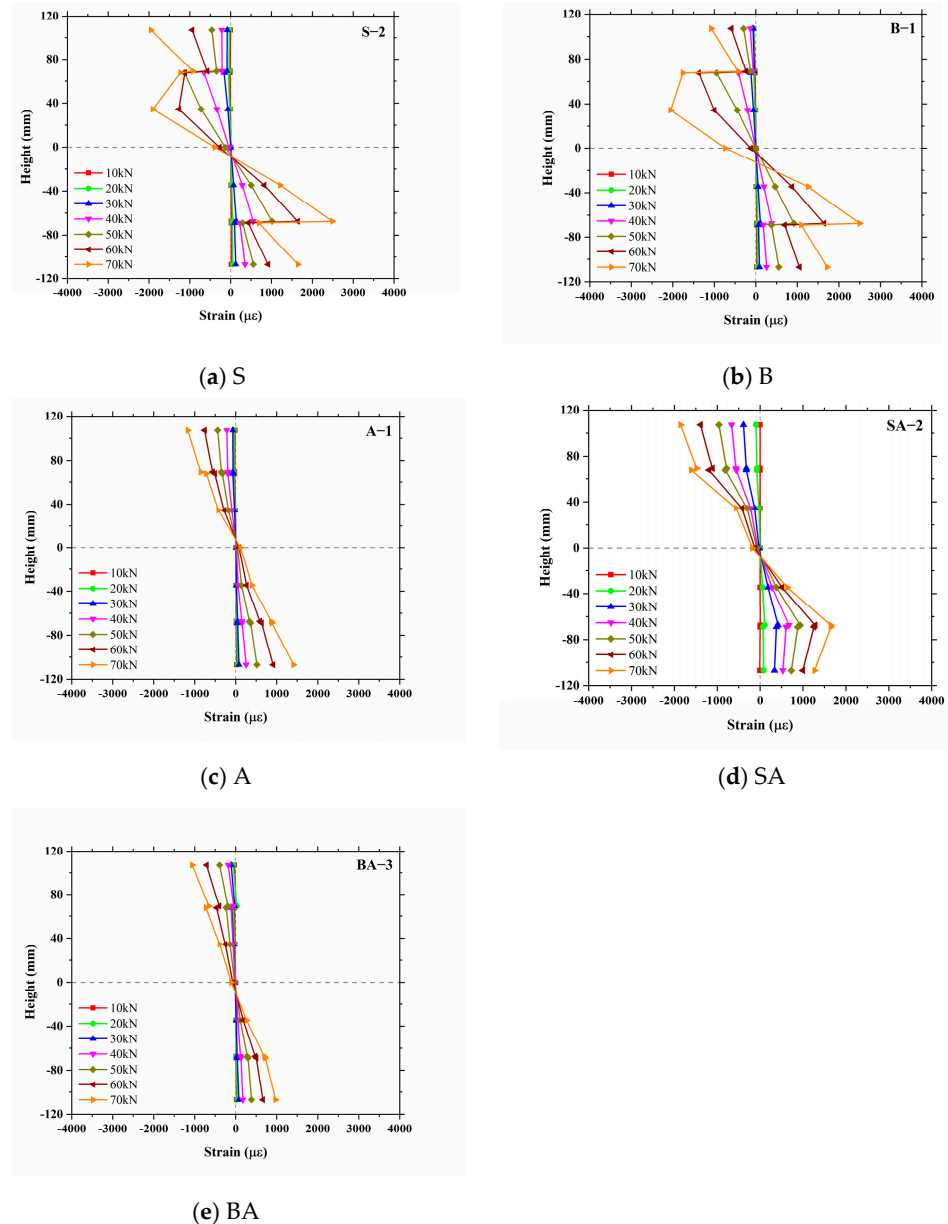


Figure 8. Strain distribution in the mid-span section of the beams.

Using specimen A-1 as an example, the excellent bonding integrity between the two was indicated by the fact that the strain of the timbers in the upper and lower flanges was roughly equivalent to the strain of the steel flanges when the load was less than 50 kN. The deformation of the steel flanges caused by compression initially damaged the adhesive layer when the load exceeded 50 kN. The strain difference became evident when the A-1 beam was loaded to 70 kN, indicating the debonding at the upper flange of the beam. However, the fact that the SA-2 beam and BA-3 beam showed a strain differential in the lower flange near the peak load suggests that the bolts and screws successfully prevented adhesive layer damage from developing. It is evident that, as the shear connection degree increased, the neutral axis in the steel deviated to the top of the section, increasing the tensile stress at the

timber edge of the lower flanges and, consequently, the timber's contribution [34]. Lastly, the beam's peak bearing capacity was raised. In groups B and S, the compression zone of the beam gradually widened as the load increased (particularly during the latter loading stage of these groups), signifying the compression yield and collapse of the timber of the upper flanges.

3.2.6. Theoretical Analysis and Verification

Table 7 compares the test and calculation values of the flexural bearing capacity. The results demonstrate that the predicted elastic and ultimate load capacities align closely with the test results. The relative error of the elastic flexural bearing capacity is less than 10%, while the relative error of the ultimate flexural bearing capacity is less than 13%. The design method is straightforward, and it can serve as a reliable reference for practical engineering design.

Table 7. Load capacity results by calculation methods.

Specimens	M_a^u kN·m	M_{exp}^u kN·m	M_a^u/M_{exp}^u	M_a^e kN·m	M_{exp}^e kN·m	M_a^e/M_{exp}^e
S	31.61	29.43	1.07	11.60	12.59	0.92
B	33.19	29.62	1.07	11.60	11.46	1.01
A-1	44.32	40.04	1.11	12.16	13.26	0.92
SA-2	46.13	47.20	0.98	12.16	10.77	1.13
BA-3	46.13	47.12	0.98	12.16	13.15	0.92

Note: M_a^u denotes the calculated ultimate bearing capacity. M_{exp}^u denotes the experimental ultimate bearing capacity. M_a^e denotes the calculated elastic bearing capacity. M_{exp}^e denotes the experimental elastic bearing capacity.

4. Conclusions

This study evaluated the bend performance of cold-formed thin-walled steel/timber composite beams to expand the use of fast-growing woods in building structures. Various connection techniques in composite beams were investigated, and the following conclusions are drawn:

1. When composite beams in Group B and Group S were tested, the timber in the upper flanges was locally squeezed or crushed, and some instances of buckling were observed on the upper flanges of the steel. Subsequently, the timber in the lower flanges broke at the midspan position. In Groups A, BA, and SA, the timber in the lower flanges fractured laterally or diagonally, accompanied by bonding failure occurring at the interface between the upper and lower flanges. The steel in the upper flanges showed no obvious yield before final failure. In Group A, the debonding of the lower flange gradually extended to the entire midspan interface. The fasteners delayed and controlled this failure in Groups BA and SA.
2. Connection methods significantly impacted the beam's flexural stiffness and load capacity. Beams connected by screws and bolts demonstrated ductile failure and an adequate ultimate bearing capacity of 74 kN. The quality of bonding significantly influenced the performance of adhesive composite beams. Specimens A-1, SA-2, and BA-3 achieved ultimate load capacities of 100 kN, 117 kN, and 117 kN, respectively, when the adhesive layer remained intact. Compared to the B and S group beams, the A group beams showed a 35% increased ultimate bearing capacity. By playing a delaying and safeguarding role, fasteners further increased the ultimate bearing capacity of SA-2 and BA-3 by approximately 18% compared to A-1. Moreover, SA-2 and BA-3 exhibited stiffness values that were 35.4% and 68.3% higher than those of Group B and S. Mechanically connected beams exhibited higher ductility than beams with glued connections.
3. During the elastic stage, the mid-span section of the composite beam exhibited a linear strain distribution at the steel-timber interface in beams connected with fasteners. As the load increased, strain differentials and slippage occurred. When adhesive was

used, the steel's strength was fully utilized, and beam slippage occurred upon damage to the adhesive layer. The proposed formula provided theoretical values for both elastic and ultimate bearing capacities that aligned well with experimental results. Compared with the experimental results, the formula demonstrated an error rate of less than 13%, mostly within 10%, indicating its applicability for the engineering design of composite beams.

4. Using hybrid connection methods like SA-2 and BA-3, composite beams exhibited significant flexural bearing capacity and stiffness. However, limitations of adhesive and hybrid connections were noted, including reduced construction efficiency and the necessity for precise operation. Environmental concerns regarding structural adhesives also present obstacles to their use. Beams with fastener connections showed improved ductility and adequate bearing capacity. It is worth emphasizing that screwed connections, which do not require pre-drilled holes, offer a more straightforward assembly process compared to bolted connections. Future research on optimizing screwed connection configurations (specifications, arrangement) is crucial for enhancing the engineering value of cold-formed thin-walled steel/timber composite beams.

Author Contributions: Conceptualization, Z.C.; methodology, J.L.; software, T.C.; validation, T.C.; formal analysis, T.C. and A.Z.; investigation, T.C.; resources, Z.C. and J.L.; data curation, T.C.; writing—original draft preparation, T.C.; writing—review and editing, J.L. and A.Z.; visualization, T.C. and A.Z.; supervision, Z.C.; project administration, Z.C.; funding acquisition, Z.C. and J.L. All authors have read and agreed to the published version of the manuscript.

Funding: This project is funded by the National Key R&D Program of China—Research on Ecological Structure System of Village Prefabricated Housing—Research on Modular Steel–timber Composite Structure System (grant No. 2019YFD1101001, Zhihua Chen).

Data Availability Statement: The data presented in this study are available on request from the corresponding author.

Acknowledgments: The support for the project is acknowledged with thanks.

Conflicts of Interest: The authors declare that they have no known competing financial interests or personal relationships that could have appeared to influence the work reported in this paper.

References

1. Khorasani, Y. Feasibility Study of Hybrid Wood Steel Structures. Master's Thesis, University of British Columbia, Vancouver, BC, Canada, 2011. Available online: <http://hdl.handle.net/2429/33561> (accessed on 23 March 2024).
2. Ghanbari Ghazijahani, T.; Jiao, H.; Holloway, D. Composite timber beams strengthened by steel and CFRP. *J. Compos. Constr.* **2017**, *21*, 04016059. [[CrossRef](#)]
3. Wang, X.; Su, P.; Liu, J.; Chen, Z.; Khan, K. Seismic performance of light steel-natural timber composite beam-column joint in low-rise buildings. *Eng. Struct.* **2022**, *256*, 113969. [[CrossRef](#)]
4. Guo, N.; Wu, M.; Li, L.; Li, G.; Zhao, Y. Bending performance of prestressed continuous glulam beams. *Adv. Civ. Eng.* **2021**, *2021*, 5512350. [[CrossRef](#)]
5. Liu, J.; Liu, R.; Li, W.; Wang, J.; Chen, L. Experimental study on the flexural performance of Timber–Steel Composite (TSC) I-beams. *Buildings* **2022**, *12*, 1206. [[CrossRef](#)]
6. Yang, H.; Liu, W.; Lu, W.; Zhu, S.; Geng, Q. Flexural behavior of FRP and steel reinforced Q glulam beams: Experimental and theoretical evaluation. *Constr. Build. Mater.* **2016**, *106*, 550–563. [[CrossRef](#)]
7. Adi, D.S.; Risanto, L.; Damayanti, R.; Rullyati, S.; Dewi, L.M.; Susanti, R.; Dwianto, W.; Hermiati, E.; Watanabe, T. Exploration of unutilized fast growing wood species from secondary forest in Central Kalimantan: Study on the fiber characteristic and wood density. *Procedia Environ. Sci.* **2014**, *20*, 321–327. [[CrossRef](#)]
8. Mola-Yudego, B.; Arevalo, J.; Díaz-Yáñez, O.; Dimitriou, I.; Freshwater, E.; Haapala, A.; Khanam, T.; Selkimäki, M. Reviewing wood biomass potentials for energy in Europe: The role of forests and fast growing plantations. *Biofuels* **2017**, *8*, 401–410. [[CrossRef](#)]
9. González-García, S.; Moreira, M.T.; Feijoo, G.; Murphy, R.J. Comparative life cycle assessment of ethanol production from fast-growing wood crops (black locust, eucalyptus and poplar). *Biomass Bioenergy* **2012**, *39*, 378–388. [[CrossRef](#)]
10. Bredemeier, M.; Busch, G.; Hartmann, L.; Jansen, M.; Richter, F.; Lamersdorf, N.P. Fast growing plantations for wood production—integration of ecological effects and economic perspectives. *Front. Bioeng. Biotechnol.* **2015**, *3*, 72. [[CrossRef](#)]

11. Kamperidou, V.; Terzopoulou, P.; Barboutis, I. Marginal lands providing tree–crop biomass as feedstock for solid biofuels. *Biofuels Bioprod. Biorefining* **2021**, *15*, 1395–1405. [[CrossRef](#)]
12. Kojima, M.; Yamamoto, H.; Okumura, K.; Ojio, Y.; Yoshida, M.; Okuyama, T.; Ona, T.; Matsune, K.; Nakamura, K.; Ide, Y. Effect of the lateral growth rate on wood properties in fast-growing hardwood species. *J. Wood Sci.* **2009**, *55*, 417–424. [[CrossRef](#)]
13. Cown, D.J. Moisture-related distortion of boards and wooden products of radiata pine: Comparison with Norway spruce. *Wood Fiber Sci.* **2005**, *37*, 424–436.
14. Montón, J.; Arriaga, F.; íñiguez-Gonzalez, G.; Segué, E. Warp requirements and yield efficiency in the visual grading of sawn radiata pine timber. *BioResources* **2015**, *10*, 1115–1126. [[CrossRef](#)]
15. Xu, P. Estimating the influence of knots on the local longitudinal stiffness in radiata pine structural timber. *Wood Sci. Technol.* **2002**, *36*, 501–509. [[CrossRef](#)]
16. Jurkiewicz, B.; Durif, S.; Bouchair, A.; Grazide, C. Experimental and analytical study of hybrid steel-timber beams in bending. *Structures* **2022**, *39*, 1231–1248. [[CrossRef](#)]
17. Jimenez, P.; Dunkl, A.; Eibel, K.; Denk, E.; Grote, V.; Kelz, C.; Moser, M. Wood or laminate?—Psychological research of customer expectations. *Forests* **2016**, *7*, 275. [[CrossRef](#)]
18. Tsai, M.T.; Le, T.D.H. Determination of initial stiffness of timber–steel composite (TSC) beams based on experiment and simulation modeling. *Sustainability* **2018**, *10*, 1220. [[CrossRef](#)]
19. Liu, R.; Liu, J.; Wu, Z.; Chen, L.; Wang, J. A study on the influence of bolt arrangement parameters on the bending behavior of timber–steel composite (TSC) beams. *Buildings* **2022**, *12*, 2013. [[CrossRef](#)]
20. Jasieńko, J.; Nowak, T.P. Solid timber beams strengthened with steel plates—Experimental studies. *Constr. Build. Mater.* **2014**, *63*, 81–88. [[CrossRef](#)]
21. Franke, S.; Franke, B.; Harte, A.M. Failure modes and reinforcement techniques for timber beams—State of the art. *Constr. Build. Mater.* **2015**, *97*, 2–13. [[CrossRef](#)]
22. De Luca, V.; Marano, C. Prestressed glulam timbers reinforced with steel bars. *Constr. Build. Mater.* **2012**, *30*, 206–217. [[CrossRef](#)]
23. Soriano, J.; Pellis, B.P.; Mascia, N.T. Mechanical performance of glued-laminated timber beams symmetrically reinforced with steel bars. *Compos. Struct.* **2016**, *150*, 200–207. [[CrossRef](#)]
24. Mcconnell, E.; Mcpolin, D.; Taylor, S. Post-tensioning of glulam timber with steel tendons. *Constr. Build. Mater.* **2014**, *73*, 426–433. [[CrossRef](#)]
25. Borri, A.; Corradi, M. Strengthening of timber beams with high strength steel cords. *Compos. Part B Eng.* **2011**, *42*, 1480–1491. [[CrossRef](#)]
26. Yang, X.; Xue, W.; Guo, N. Bending performance of glued-lumber beam reinforced with steel plate. *J. Jilin Univ. (Eng. Technol. Ed.)* **2017**, *47*, 10.
27. Bulleit, W.M.; Sandberg, L.B.; Woods, G.J. Steel reinforced glued laminated timber. *J. Struct. Eng.* **1989**, *115*, 433–444. [[CrossRef](#)]
28. Wang, Y.; Hou, Q.; Xu, T.; Qu, S.; Zhang, B. The bending-shear behaviors of steel reinforced fast-growing poplar glulam beams with different shear-span ratios. *Constr. Build. Mater.* **2021**, *300*, 124008. [[CrossRef](#)]
29. Bulleit, W. Reinforcement of wood materials: A review. *Wood Fiber Sci.* **1984**, *16*, 391–397.
30. Fajdiga, G.; Šubic, B.; Kovačič, A. Bending stiffness of hybrid wood-metal composite beams: An experimentally validated numerical model. *Forests* **2021**, *12*, 918. [[CrossRef](#)]
31. Šubic, B.; Fajdiga, G.; Lopatič, J. Bending stiffness, load-bearing capacity and flexural rigidity of slender hybrid wood-based beams. *Forests* **2018**, *9*, 703. [[CrossRef](#)]
32. Winter, W.; Tavoussi, K.; Pixner, T.; Parada, F.R. Timber-steel-hybrid beams for multi-storey buildings: Final report. In Proceedings of the World Conference on Timber Engineering 2016, Vienna, Austria, 22–25 August 2016.
33. Kyvelou, P.; Gardner, L.; Nethercot, D.A. Composite action between cold-formed steel beams and wood-based floorboards. *Int. J. Struct. Stab. Dyn.* **2015**, *15*, 1540029. [[CrossRef](#)]
34. Kyvelou, P.; Gardner, L.; Nethercot, D.A. Testing and analysis of composite cold-formed steel and wood–based flooring systems. *J. Struct. Eng.* **2017**, *143*, 04017146. [[CrossRef](#)]
35. Hassanieh, A.; Valipour, H.R.; Bradford, M.A. Experimental and numerical study of steel-timber composite (STC) beams. *J. Constr. Steel Res.* **2016**, *122*, 367–378. [[CrossRef](#)]
36. Hassanieh, A.; Valipour, H.R.; Bradford, M.A. Experimental and numerical investigation of short-term behaviour of CLT-steel composite beams. *Eng. Struct.* **2017**, *144*, 43–57. [[CrossRef](#)]
37. Kyvelou, P.; Gardner, L.; Nethercot, D.A. Finite element modelling of composite cold-formed steel flooring systems. *Eng. Struct.* **2018**, *158*, 28–42. [[CrossRef](#)]
38. Kyvelou, P.; Reynolds, T.P.S.; Beckett, C.T.S.; Huang, Y. Experimental investigation on composite panels of cold-formed steel and timber. *Eng. Struct.* **2021**, *247*, 113186. [[CrossRef](#)]
39. Kyvelou, P.; Gardner, L.; Nethercot, D.A. Design of composite cold-formed steel flooring systems. *Structures* **2017**, *12*, 242–252. [[CrossRef](#)]
40. Kyvelou, P.; Gardner, L.; Nethercot, D.A. Impact statement on “design of composite cold-formed steel flooring systems”. *Structures* **2019**, *20*, 213. [[CrossRef](#)]
41. Awadhani, L.V.; Bewoor, A. Parametric study of single bolted composite bolted joint subjected to static tensile loading. *IOP Conf. Series. Mater. Sci. Eng.* **2017**, *225*, 12215. [[CrossRef](#)]

42. Dujmovic, D.; Androic, B.; Lukacevic, I. *Composite Structures According to Eurocode 4, Worked Examples*; Ernst & Sohn: Berlin, Germany, 2015.
43. Hassanieh, A.; Valipour, H.R.; Bradford, M.A. Load-slip behaviour of steel-cross laminated timber (CLT) composite connections. *J. Constr. Steel. Res.* **2016**, *122*, 110–121. [[CrossRef](#)]
44. Hassanieh, A.; Valipour, H.R.; Bradford, M.A. Composite connections between CLT slab and steel beam: Experiments and empirical models. *J. Constr. Steel. Res.* **2017**, *138*, 823–836. [[CrossRef](#)]
45. Loss, C.; Piazza, M.; Zandonini, R. Connections for steel–timber hybrid prefabricated buildings. Part I: Experimental tests. *Constr. Build. Mater.* **2016**, *122*, 781–795. [[CrossRef](#)]
46. Hassanieh, A.; Valipour, H.R.; Bradford, M.A. Experimental and analytical behaviour of steel-timber composite connections. *Constr. Build. Mater.* **2016**, *118*, 63–75. [[CrossRef](#)]
47. Vella, N.; Gardner, L.; Buhagiar, S. Experimental analysis of cold-formed steel-to-timber connections with inclined screws. *Structures* **2020**, *24*, 890–904. [[CrossRef](#)]
48. Yang, R.; Li, H.; Lorenzo, R.; Ashraf, M.; Sun, Y.; Yuan, Q. Mechanical behaviour of steel timber composite shear connections. *Constr. Build. Mater.* **2020**, *258*, 119605. [[CrossRef](#)]
49. Chen, Z.; Niu, X.; Liu, J.; Khan, K. Experimental study of thin-walled steel-timber single-shear connection with a self-tapping screw. *Structures* **2021**, *34*, 4389–4405. [[CrossRef](#)]
50. Zhang, A.; Liu, J.; Wang, J.; Chen, Z.; Li, Y. Experimental and analytical behaviour of light gauge steel-fast growing timber composite shear connections. *Structures* **2023**, *47*, 1691–1709. [[CrossRef](#)]
51. Liu, J.; Zhang, A.; Chen, Z.; Liu, Y.; Li, Y. Experimental and theoretical model study on the shear behavior of the self-tapping screw connections of steel-timber composite members. *J. Tianjin Univ. (Sci. Technol.)* **2023**, *56*, 680–689.
52. *GB/T 228.1-2021; Metallic Materials—Tensile Testing—Part 1: Method of Test at Room Temperature*. Standardization Administration of China: Beijing, China, 2019.
53. *GB50005-2017; Standard for Design of Timber Structures*. Ministry of Housing and Urban-Rural Development of the People’s Republic of China: Beijing, China, 2017.
54. *GB/T 1943-2009; Method for Determination of the Modulus of Elasticity in Compression Perpendicular to Grain of Wood*. General Administration of Quality Supervision, Inspection and Quarantine of the People’s Republic of China: Beijing, China, 2009.
55. *GB/T 1939-2009; Method of Testing in Compression Perpendicular to Grain of Wood*. General Administration of Quality Supervision, Inspection and Quarantine of the People’s Republic of China: Beijing, China, 2009.
56. *GB/T 15777-2017; Method for Determination of the Modulus of Elasticity in Compression Parallel to Grain of Wood*. General Administration of Quality Supervision, Inspection and Quarantine of the People’s Republic of China: Beijing, China, 2017.
57. *GB-T 1928-2009; General Request for Physical and Mechanical Test for Wood*. Ministry of Forestry of the PRC: Beijing, China, 2009.
58. *GB/T 50329-2012; Standard for Test Methods of Timber Structures*. Housing and Urban-Rural Development of the People’s Republic of China: Beijing, China, 2012.
59. Zhou, H. Flagship Store of Ailike. Available online: <https://ailikebg.tmall.com> (accessed on 23 March 2024).
60. Zhang, F.; Chen, H.; Li, X.; Li, H.; Lv, T.; Zhang, W.; Yang, Y. Experimental study of the mechanical behavior of FRP-reinforced concrete canvas panels. *Compos. Struct.* **2017**, *176*, 608–616. [[CrossRef](#)]
61. Li, H.; Chen, H.; Li, X.; Zhang, F. Design and construction application of concrete canvas for slope protection. *Powder Technol.* **2019**, *344*, 937–946. [[CrossRef](#)]
62. Chen, T.; Chen, Z.; Liu, J. Experimental and numerical analysis of single-strap adhesive joints combining thin-walled steel and fast-growing natural timber. *Int. J. Adhes. Adhes.* **2023**, *126*, 103434. [[CrossRef](#)]
63. *GJB 715.24 A 2002; Fastener Test Methods-Single Shear*. Commission of Science, Technology and Industry for National Defense: Beijing, China, 2002.
64. *GB/T 232-2010; Metallic Materials-Bend Test*. Ministry of Housing and Urban-Rural Development of the People’s Republic of China: Beijing, China, 2011.
65. Hassanieh, A.; Valipour, H.R.; Bradford, M.A.; Sandhaas, C. Modelling of steel-timber composite connections: Validation of finite element model and parametric study. *Eng. Struct.* **2017**, *138*, 35–49. [[CrossRef](#)]
66. Chybiński, M.; Polus, Ł. Experimental and numerical investigations of aluminium-timber composite beams with bolted connections. *Structures* **2021**, *34*, 1942–1960. [[CrossRef](#)]
67. Li, Y.; Shan, W.; Shen, H.; Zhang, Z.; Liu, J. Bending resistance of I-section bamboo–steel composite beams utilizing adhesive bonding. *Thin-Walled Struct.* **2015**, *89*, 17–24. [[CrossRef](#)]
68. Duan, S.; Zhou, W.; Liu, X.; Yuan, J.; Wang, Z.; Cristiano, L.; Loss, C. Experimental study on the bending behavior of steel-wood composite beams. *Adv. Civ. Eng.* **2021**, *2021*, 1315849. [[CrossRef](#)]
69. Shan, Q.; Zhang, J.; Tong, K.; Li, Y.; Dongsheng, H.; Huang, D. Study on flexural behaviour of box section bamboo-steel composite beams. *Adv. Civ. Eng.* **2020**, *2020*, 8878776. [[CrossRef](#)]
70. Duan, Y.; Zhang, J.; Tong, K.; Wu, P.; Li, Y. The effect of interfacial slip on the flexural behavior of steel-bamboo composite beams. *Structures* **2021**, *32*, 2060–2072. [[CrossRef](#)]

71. Feng, P.; Qiang, H.-L.; Ye, L.-P. Discussion and definition on yield points of materials, members and structures. *Eng. Mech.* **2017**, *34*, 36–46.
72. Gao, Y.; Xu, F.; Meng, X.; Zhang, Y.; Yang, H. Experimental and numerical study on the lateral torsional buckling of full-scale steel-timber composite beams. *Adv. Struct. Eng.* **2022**, *25*, 522–540. [[CrossRef](#)]

Disclaimer/Publisher’s Note: The statements, opinions and data contained in all publications are solely those of the individual author(s) and contributor(s) and not of MDPI and/or the editor(s). MDPI and/or the editor(s) disclaim responsibility for any injury to people or property resulting from any ideas, methods, instructions or products referred to in the content.